

From the earliest seeds to today's supermassive black holes

Piero Madau

Department of Astronomy and Astrophysics, University of California, Santa Cruz CA 95064, USA

Abstract. I review scenarios for the assembly of supermassive black holes (MBHs) at the center of galaxies that trace their hierarchical build-up far up in the dark matter halo “merger tree”. Monte Carlo realizations of the merger hierarchy in a Λ CDM cosmology, coupled to semi-analytical recipes, are a powerful tool to follow the merger history of halos and the dynamics and growth of the MBHs they host. X-ray photons from mini-*quasars* powered by intermediate-mass “seed” holes may permeate the universe more uniformly than EUV radiation, make the low-density diffuse intergalactic medium warm and weakly ionized prior to the epoch of reionization breakthrough, and set an entropy floor. The spin distribution of MBHs is determined by gas accretion, and is predicted to be heavily skewed towards fast-rotating Kerr holes, already in place at early epochs, and not to change significantly below redshift 5. Decaying MBH binaries may shape the innermost central regions of galaxies and should be detected in significant numbers by *LISA*.

1 Massive black holes and galaxy formation

The strong link observed between the masses of supermassive black holes (MBHs) at the center of most galaxies and the gravitational potential wells that host them suggests a fundamental mechanism for assembling black holes and forming spheroids in galaxy halos. The $m_{\text{BH}}-\sigma$ relation [12] [16] implies a rough proportionality between MBH mass and the mass of the baryonic component of the bulge. It is not yet understood whether this relation was set in primordial structures, and consequently how it is maintained throughout cosmic time with such a small dispersion, or indeed which physical processes established such a correlation in the first place [48][18][6].

In cosmologies dominated by cold dark matter (CDM) galaxy halos experience multiple mergers during their lifetime, with those between comparable-mass systems (“major mergers”) expected to result in the formation of elliptical galaxies [21]. Simple models in which MBHs are also assumed to grow during major mergers and to be present in every galaxy at any redshift – while only a fraction of them is “active” at any given time – have been shown to explain many aspects of the observed evolution of quasars [7][8][25]. The coevolution of MBHs and their host galaxies in hierarchical structure formation scenarios gives origin to a number of of important questions, most notably:

- *Did the first MBHs form in subgalactic units far up in the merger hierarchy, well before the bulk of the stars observed today?* The seeds of the $z \sim 6$ quasars

discovered in the *Sloan Digital Sky Survey* had to appear at very high redshift, $z \gtrsim 10$, if they are accreting no faster than the Eddington rate. In hierarchical cosmologies, the ubiquity of MBHs in nearby luminous galaxies can arise even if only a small fraction of halos harbor MBHs at very high redshift [32].

- *How massive were the initial seeds, and is there a population of relic pre-galactic MBHs lurking in present-day galaxy halos?* A clue to these questions may lie in the numerous population of ultraluminous off-nuclear (“non-AGN”) X-ray sources that have been detected in nearby galaxies [34]. Assuming isotropic emission, the inferred masses of these “ULXs” may suggest intermediate-mass black holes with masses \gtrsim a few hundred M_\odot [9][24].

- *Can coalescing MBH binaries at very high redshift be detected in significant numbers by the planned Laser Interferometer Space Antenna (LISA)?* If MBHs were common in the past (as implied by the notion that many distant galaxies harbor active nuclei for a short period of their life), and if their host galaxies undergo multiple mergers, then MBH binaries will inevitably form in large numbers during cosmic history. MBH pairs that are able to coalesce in less than a Hubble time will give origin to the loudest gravitational wave events in the universe.

- If was first proposed by [10] that the heating of the surrounding stars by a decaying MBH pair would create a low-density core out of a preexisting cuspy (e.g. $\rho_* \propto r^{-2}$) stellar density profile. If stellar dynamical processes can efficiently drive wide MBH binaries to the gravitational wave (GW) emission stage, *what is the cumulative dynamical effect of multiple black hole mergers on galaxy stellar cusps?*

- Active galactic nuclei powered by supermassive holes keep the universe ionized at $z \lesssim 4$, structure the intergalactic medium (IGM), and probably regulate star formation in their host galaxies. Intermediate-mass holes accreting gas from the surrounding medium may shine as “miniquasars” at redshifts as high as $z \sim 20$. *What is the thermodynamic effect of miniquasars on the IGM at early times?*

- Besides their masses, astrophysical black holes are completely characterized by their spins, $S = aGm_{\text{BH}}/c$, $0 \leq a/m_{\text{BH}} \leq 1$. The spin of a MBH is expected to have a significant effect on its observational manifestation, such as the efficiency of converting accreted mass into radiation and the existence and direction of jets in active nuclei. *What is the expected distribution of MBH spins and how does this evolve with cosmic time?*

In this talk I will review some recent developments in our understanding of the assembly, growth, emission history, and environmental impact of MBHs from early epochs to the present. Unless otherwise stated, all the results shown below refer to the currently favoured (by a variety of observations) Λ CDM world model with $\Omega_M = 0.3$, $\Omega_\Lambda = 0.7$, $h = 0.7$, $\Omega_b = 0.045$, $\sigma_8 = 0.93$, and $n = 1$.

2 MBHs as Population III remnants

The first stars in the universe must have formed out of metal-free gas, in dark matter “minihalos” of total mass $\gtrsim 5 \times 10^5 M_\odot$ [14] condensing from the high- σ peaks of the primordial density field at redshift $z = 20 - 30$. Numerical simulations of the fragmentation of primordial clouds in standard CDM theories all show the formation of Jeans unstable clumps with masses exceeding a few hundred solar masses; because of the slow subsonic contraction – a regime set up by the main gas coolant, molecular hydrogen – further fragmentation into sub-components is not seen, and a single very massive star forms from the inside out [5][1][41].

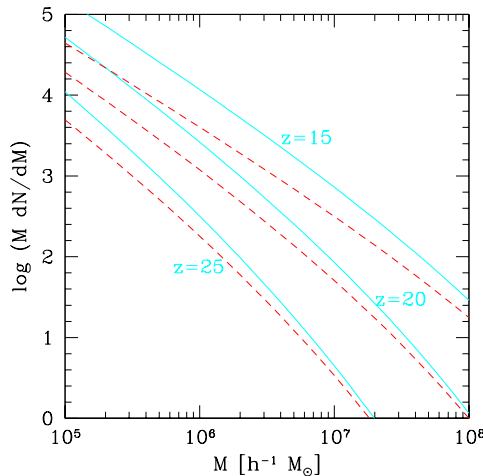


Fig. 1. Mass function of minihalos of mass M formed at $z = 15, 20, 25$ which, by the later time z_0 , will have merged into a more massive halo of total mass M_0 . *Solid curves*: $z_0 = 0.8$, $M_0 = 10^{12} h^{-1} M_\odot$ (“Milky Way” halo). *Dashed curves*: $z_0 = 3.5$, $M_0 = 2 \times 10^{11} h^{-1} M_\odot$ (older “bulge”). If only one seed hole formed in each $\sim 10^6 M_\odot$ minihalo collapsing at $z \sim 20$ (and triple hole interactions and binary coalescences were neglected), several thousands relic IMBHs and their descendants would be orbiting throughout present-day galaxy halos [29][23].

At zero metallicity mass loss through radiatively-driven stellar winds or nuclear-powered stellar pulsations is expected to be negligible, and Population III stars will likely die losing only a small fraction of their mass (except for $100 < m_* < 140 M_\odot$). Nonrotating very massive stars in the mass window $140 \lesssim m_* \lesssim 260 M_\odot$ will disappear as pair-instability supernovae [4], leaving no compact remnants and polluting the universe with the first heavy elements [44][40]. Stars with $40 < m_* < 140 M_\odot$ and $m_* > 260 M_\odot$ are predicted instead to collapse to black holes with masses exceeding half of the initial stellar

mass [20]. Barring any fine tuning of the initial mass function of Pop III stars, intermediate-mass black holes (IMBHs) – with masses above the 4–18 M_{\odot} range of known “stellar-mass” holes – may then be the inevitable endproduct of the first episodes of pregalactic star formation [29]. Since they form in high- σ rare density peaks, relic IMBHs are expected to cluster in the bulges of present-day galaxies as they become incorporated through a series of mergers into larger and larger systems (see Fig. 1). The presence of a small cluster of IMBHs in galaxy nuclei may have several interesting consequences associated with tidal captures of ordinary stars (likely followed by disruption), capture by the central supermassive hole, and gravitational wave radiation from such coalescences [33]. Accreting pregalactic IMBHs may be detectable as ultra-luminous, off-nuclear X-ray sources [29][26].

3 The first miniquasars

Physical conditions in the central potential wells of young and gas-rich protogalaxies may have been propitious for black hole gas accretion. Perhaps seed black holes grew efficiently in small minihalos just above the cosmological Jeans mass (with shallow potential wells), or maybe gas accretion had to await the buildup of more massive galaxies (with virial temperatures above the threshold for atomic cooling). This issue is important for the detectability of high- z miniquasars: it also determines whether the radiation background at very high redshifts had an X-ray component able to preheat and partially ionize the IGM.

As mentioned above, gas condensation in the first baryonic objects is possible through the formation of H_2 molecules, which cool via roto-vibrational transitions down to temperatures of a few hundred kelvins. In the absence of a UV photodissociating flux and of ionizing X-ray radiation, three-dimensional simulations of early structure formation show that the fraction of cold, dense gas available for accretion onto seed holes or star formation exceeds 20% for halos more massive than $10^6 M_{\odot}$ [28]. On the other hand, a zero-metallicity progenitor star in the range $40 < m_* < 500 M_{\odot}$ emits about 70,000 photons above 1 ryd per stellar baryon [43]. The ensuing ionization front will completely overrun the host halo, photoevaporating most of the surrounding gas [54]. Black hole remnants of the first stars that created $H\,\text{II}$ regions are then unlikely to accrete significant mass until new cold material will be made available through the hierarchical merging of many gaseous subunits.

Accretion onto IMBHs may be an attractive way to (partially) reionize the low-density IGM [30][42]. A large fraction of the UV radiation from massive stars may not escape the dense sites of star formation, or may be deposited locally in halo gas that recombines almost immediately. The harder radiation emitted from miniquasars is instead more likely to escape from the hosts into intergalactic space, and may then produce more ‘durable’ (albeit partial) ionization in the diffuse IGM. High-resolution hydrodynamics simulations of early structure formation in Λ CDM cosmologies are a powerful tool to track in de-

tail the thermal and ionization history of a clumpy IGM and guide studies of early reheating. We [27] have used *Enzo*, an adaptive mesh refinement (AMR), grid-based hybrid (hydro+N-body) code developed by Bryan & Norman (see <http://cosmos.ucsd.edu/enzo/>) to solve the cosmological hydrodynamics equations and simulate the effect of a miniquasar turning on at very high redshift in a volume 1 Mpc on a side (comoving). We first identify in a low-resolution pure N-body simulation the Lagrangian volume of a resolved protogalactic halo with a total mass $7 \times 10^5 M_\odot$ at $z = 25$, above the cosmological Jeans mass. We then generate new initial conditions with an 128^3 initial static grid that covers a 0.5 Mpc volume centered around the identified high- σ peak. During the evolution, refined grids (for a maximum of 5 additional levels) are introduced with twice the spatial resolution of the parent (coarser) grid to home in, with progressively finer resolution, on the densest parts of the “cosmic web”. The simulation follows the non-equilibrium chemistry of the dominant nine species (H , H^+ , H^- , e , He , He^+ , He^{++} , H_2 , and H_2^+) in primordial gas, and includes radiative losses from atomic and molecular line cooling.

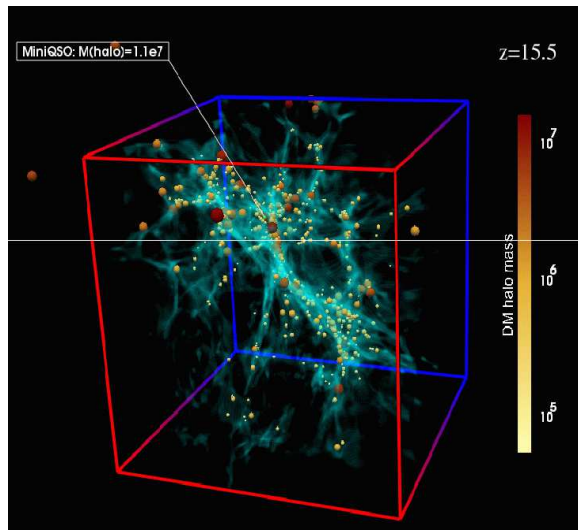


Fig. 2. Gas distribution (at overdensity 2) in the inner 0.5 Mpc of the simulation box at $z = 15.5$. Dark matter halos of different masses (identified with a halo-finder algorithm) are plotted as dark spheres.

At $z = 21$, a miniquasar powered by a $150 M_\odot$ black hole accreting at the Eddington rate is turned on in the protogalactic halo. The miniquasar shines for a few Salpeter times (i.e. down to $z \sim 15$) and is a copious source of soft X-ray photons, which permeate the IGM more uniformly than possible with extreme ultraviolet (EUV, ≥ 13.6 eV) radiation [38] and make it warm and weakly ionized prior to the epoch of reionization breakthrough [50]. A spectrum with $\nu L_\nu = \text{const}$ (like the nonthermal component observed in ULXs) was assumed for photons with energies in the range 0.2-10 keV, to which the simulation box is

transparent. X-rays alone do not produce a fully ionized medium, but partially photoionize the gas by repeated secondary ionizations. A primary nonthermal photoelectron of energy $E = 1$ keV in a medium with residual ionization (from the recombination epoch) $x = 2 \times 10^{-4}$ will create over two dozens secondary electrons, depositing a fraction $f_{\text{ion}} \approx 37\%$ of its initial energy as secondary ionizations of hydrogen, and only $f_{\text{heat}} \approx 13\%$ as heat [47]. The timescale for electron-electron encounters resulting in a fractional energy loss $f = \Delta E/E$,

$$t_{\text{ee}} \approx 140 \text{ yr } Ef \left(\frac{1+z}{20} \right)^{-3} \left(\frac{\ln A}{20} \right)^{-1} x^{-1} \quad (1)$$

(where E is measured in keV), is typically much shorter than the electron Compton cooling timescale off cosmic microwave background (CMB) photons, $t_C = (7 \times 10^6 \text{ yr})[(1+z)/20]^{-4}$, and thus the primary photoelectron will ionize and heat the surrounding medium before it is cooled by the CMB. Once the IGM ionized fraction increases to $x \approx 0.1$, the number of secondary ionizations per ionizing photon drops to a few, and the bulk of the primary's energy goes into heat ($f_{\text{heat}} \approx 0.6$) via elastic Coulomb collisions with thermal electrons.

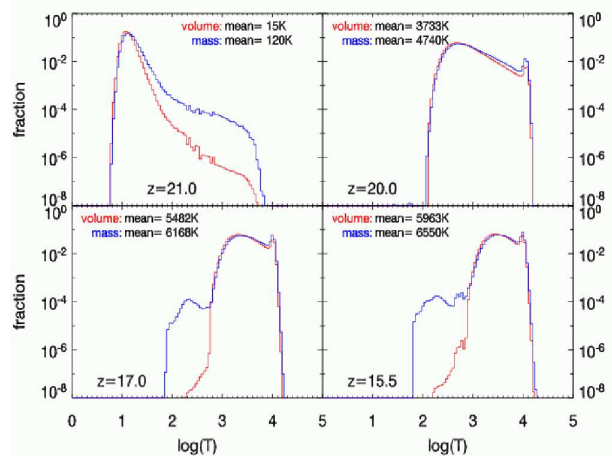


Fig. 3. Mass (upper curves) and volume (lower curves) weighted gas fraction vs. gas temperature in the simulation box. A miniquasar was turned on at $z = 21$.

Figure 3 shows the mass and volume-weighted gas fraction in the simulation box vs. temperature as four different redshifts. The heating effect of X-rays from the miniquasar is clearly seen, with gas temperatures between 10^3 and 10^4 K at $z < 20$. Strong Jeans mass filtering takes place, and subsequent minihalos will no longer be able to accrete gas due to the smoothing effect of gas pressure. The low-density IGM acquires a uniform “entropy floor” [39] that (a) greatly reduces gas clumping, curtailing the number of photons needed to maintain reionization, and (b) results in significantly lower gas densities in the cores of minihalos that

suppress rapid H₂ formation. The latter effect may imply that X-rays inhibit rather than enhance star formation [19][28].

4 MBH binaries and galaxy cores

Frequent galaxy mergers will inevitably lead to the formation of MBH binaries. As dark matter halos assemble, MBHs get incorporated into larger and larger halos, sink to the center owing to dynamical friction, accrete a fraction of the gas in the merger remnant to become supermassive, form a binary system, and eventually coalesce [3]. In a stellar background a “hard” binary shrinks by capturing the stars that pass close to the holes and ejecting them at much higher velocities, a super-elastic scattering process that depletes the nuclear region and turns a stellar “cusp” into a low-density core. Rapid coalescence eventually ensues due to the emission of gravitational radiation. Observationally, there is clear evidence in early-type galaxies for a systematic trend in the distribution of surface brightness profiles, with faint ellipticals showing steep power-law profiles (cusps), while bright ellipticals have much shallower stellar cores [11]. Detailed N-body simulations have confirmed the cusp-disruption effect of a hardening MBH binary [35], but have shed little light on why bright ellipticals have lower central concentrations than faint ellipticals.

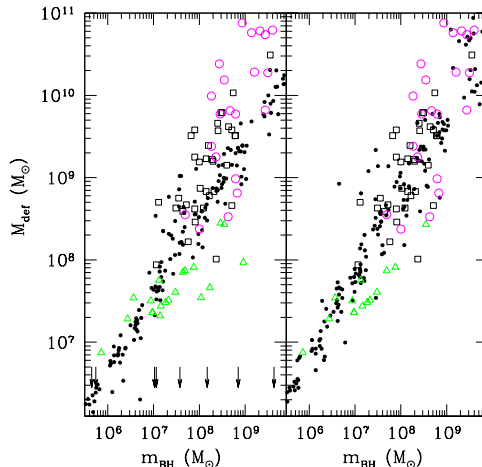


Fig. 4. Mass deficit produced at $z = 0$ by shrinking MBHs in our merger tree as a function of nuclear MBH mass (*filled dots*). *Left panel*: cusp regeneration case. *Right panel*: core preservation case. Galaxies without a core (i.e. those that have never experienced a MBH-MBH merger or with their cusp recently regenerated) are shown as vertical arrows at an arbitrary mass deficit of $10^6 M_\odot$. *Empty squares*: mass deficit inferred in a sample of galaxies by [36]. *Empty circles*: same for the “core” galaxies of [11]. *Empty triangles*: same for the “cuspy” galaxies of [11], assuming a flat core within the upper limit on the core size. (From [52].)

The role of MBH binaries in shaping the central structure of galaxies is best understood within the framework of a detailed model for the hierarchical assembly of MBHs over cosmic history [51]. Stellar cusps can be efficiently destroyed over cosmic time by decaying binaries if stellar dynamical processes are able to shrink the binary down to a separation $\lesssim 10\%$ of the separation at which the binary becomes hard. More massive halos have more massive nuclear holes and experience more merging events than less massive galaxies: hence they suffer more from the eroding action of binary MBHs and have larger cores. In [52] we found that a model in which the effect of the hierarchy of MBH interactions is cumulative and cores are preserved during galaxy mergers produces at the present epoch a correlation between the “mass deficit” (the mass needed to bring a flat inner density profile to a r^{-2} cusp) and the mass of the nuclear MBH, with a normalization and slope comparable to the observed relation (see Fig. 4). Models in which the mass displaced by the MBH binary is replenished after every major galaxy merger appear instead to underestimate the mass deficit observed in “core” galaxies. In [52] a simple scheme was applied to hardening pairs, in which the “loss cone” is constantly refilled and a constant density core forms due to the ejection of stellar mass. The effect of loss-cone depletion (the depletion of low-angular momentum stars that get close enough to extract energy from a hard binary) is one of the major uncertainties in computing the decay timescale, and makes it difficult to construct detailed scenarios for coalescing black hole binaries.

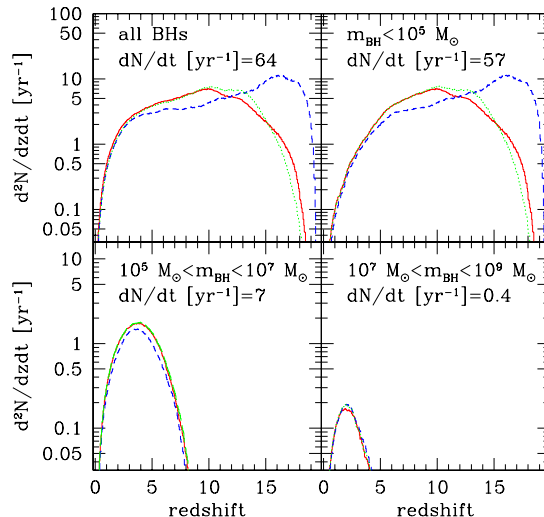


Fig. 5. Number of MBH binary coalescences observed per year at $z = 0$, per unit redshift, in different $m_{\text{BH}} = M_1 + M_2$ mass intervals. Each panel also lists the integrated event rate, dN/dt , predicted by [45]. The rates (solid lines) are compared to a case in which triple black hole interactions are switched off (dotted lines). Triple hole interac-

tions increase the coalescence rate at very high redshifts, while, for $10 < z < 15$, the rate is decreased because of the reduced number of surviving binaries. *Dashed lines*: rates computed assuming binary hardening is instantaneous, i.e. MBHs coalesce after a dynamical friction timescale.

5 Gravitational radiation from inspiraling MBH binaries

MBH binaries, with masses in the range $10^3 - 10^7 M_\odot$, are one of the primary target for *LISA* [17][55][45]. Interferometers operate as all-sky monitors, and the data streams collect the contributions from a large number of sources belonging to different cosmic populations. To optimize the subtraction of resolved sources from the data stream, it is important to have a detailed description of the expected rate, duration, amplitude, and waveforms of events. Figure 5 shows the number of MBH binary coalescences per unit redshift per unit *observed* year predicted by [45], using a detailed model of MBH binaries dynamics. The observed event rate is obtained by dividing the rate per unit proper time by the $(1+z)$ cosmological time dilation factor. Each panel shows the rate for different $m_{\text{BH}} = M_1 + M_2$ mass intervals, and lists the integrated event rate, dN/dt , across the entire sky. The number of events per observed year per unit redshift peaks at $z = 2$ for $10^7 < m_{\text{BH}} < 10^9 M_\odot$, at $z = 3 - 4$ for $10^5 < m_{\text{BH}} < 10^7 M_\odot$, and at $z = 10$ for $m_{\text{BH}} < 10^5 M_\odot$, i.e. the lower the black hole mass, the higher the peak redshift. Beyond the peak, the event rate decreases steeply with cosmic time.

In the stationary case, i.e., assuming no orbital decay, the GW emission spectrum of a MBH pair in a circular orbit of radius a is a delta function at rest-frame frequency $f_r = \omega/\pi$, where $\omega = \sqrt{G(M_1 + M_2)/a^3}$ is the Keplerian angular frequency of the binary. Orbital decay due to GW emission results in a shift of the emitted frequency to increasingly larger values as the binary evolution proceeds. Typically, the timescale for frequency shift is long compared to the wave period, and short compared to the duration of the observation. Only close to the innermost stable circular orbit (ISCO), the GW frequency changes at a rate comparable to the frequency itself. The rest-frame energy flux (energy per unit area per unit time) associated to the GW is

$$\frac{dE}{dAdt} = \frac{\pi c^3}{4 G} f_r^2 h^2, \quad (2)$$

where the strain amplitude (sky-and-polarisation averaged) at comoving distance $r(z)$ is

$$h = \frac{8\pi^{2/3}}{10^{1/2}} \frac{G^{5/3} \mathcal{M}^{5/3}}{c^4 r(z)} f_r^{2/3}, \quad (3)$$

\mathcal{M} is the “chirp mass” of the binary, and all the other symbols have their standard meaning. The strain is averaged over a wave period. The important quantity to consider is the number of cycles n spent in a frequency interval $\Delta f \simeq f$ around a given frequency f . In general, $n = f^2/\dot{f} \propto f^{-5/3}$. For a periodic signal

at frequency f lasting for a time interval longer than the observation time τ , we have simply $n = f\tau$. The characteristic strain in an observation of (observed) duration τ is then

$$h_c = h\sqrt{n} \propto f_r^{-1/6}, \quad n < f\tau, \quad (4)$$

and

$$h_c = h\sqrt{f\tau} \propto f_r^{7/6}, \quad n > f\tau, \quad (5)$$

where $f = f_r/(1+z)$ is the observed frequency. In Figure 6 h_c is plotted for different MBH binaries at different redshifts, compared to the *LISA* h_{rms} multiplied by a factor of 5, assuming a 3-year observation.

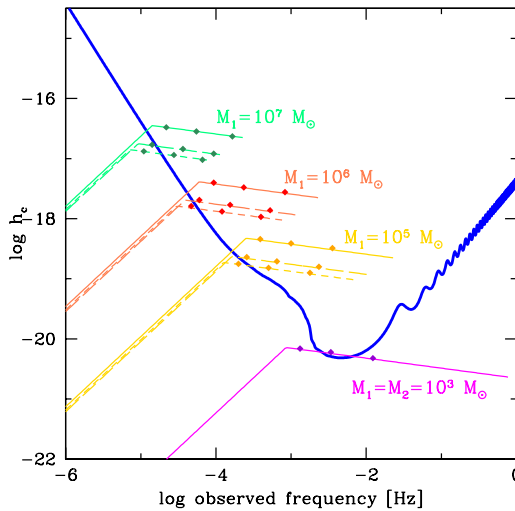


Fig. 6. Characteristic strain h_c for MBH binaries with different masses and redshifts. From top to bottom, the first three curves refer to systems with $\log(M_1/M_\odot) = 7, 6, 5$, respectively, and $M_2 = 0.1M_1$. The solid, long-dashed, and short-dashed lines assume the binary at $z = 1, 3, 5$, respectively. A 3-year observation is considered. The lowest solid curve assumes an equal mass binary $M_1 = M_2 = 10^3 M_\odot$ at $z = 7$. The small diamonds on each curve mark, from left to right, the observed frequency at 1 year, 1 month and 1 day before coalescence. The thick curve is *LISA* $5h_{\text{rms}}$, approximatively the threshold for detection with $S/N \geq 5$. (From [46]).

At frequencies higher than the “knee”, the time spent around a given frequency is less than 3 years, and $h_c \propto f^{-1/6}$. The signal shifts toward higher frequency during the observation, and reaches the ISCO and the coalescence phase in most cases. The lowest curve represents a low mass, high redshift equal mass binary. In terms of their detectability by *LISA*, they represent a somewhat different class of events. Contrary to the case of more massive binaries present at lower z , the final coalescence phase of light binaries lies at too high frequencies, well below the *LISA* threshold. For frequencies much below the knee, the characteristic strain is proportional to $f^{7/6}$, as the timescale for frequency shift

is longer than 3 years. The signal amplitude is then limited by the observation time, not by the intrinsic properties of the source. The source will be observed as a “stationary source”, a quasi-monochromatic wave for the whole duration of the observation. An increase in the observation time will result in a shift of the knee toward lower frequencies. The time needed for the sources to reach the ISCO starting from the knee frequency is, approximatively, the observing time.

As recently shown by [46], the GW signal from MBH binaries will be resolved (assuming a 3-year *LISA* observation) into ~ 100 discrete events, 40 of which will be observed above threshold until coalescence. These “merging events” involve relatively massive binaries, $M \sim 10^5 M_\odot$, in the redshift range $2 \lesssim z \lesssim 6$. The remaining ~ 60 events come from higher redshift, less massive binaries ($M \sim 5 \times 10^3 M_\odot$ at $z \gtrsim 6$) and, although their S/N integrated over the duration of the observation can be substantial, the final coalescence phase is at too high frequency to be directly observable by *LISA*. The total number of detected events accounts for a fraction $\gtrsim 90\%$ of all coalescences of massive black hole binaries at $z \lesssim 5$. The residual confusion noise from unresolved massive black hole binaries is expected to be at least an order of magnitude below the estimated stochastic *LISA* noise.

6 MBH spins

The spin of a MBH is determined by the competition between a number of physical processes. Black holes forming from the gravitational collapse of very massive stars endowed with rotation will in general be born with non-zero spin [13]. An initially non-rotating hole that increases its mass by (say) 50% by swallowing material from an accretion disk may be spun up to $a/m_{\text{BH}} = 0.84$ [2]. While the coalescence of two non-spinning black holes of comparable mass will immediately drive the spin parameter of the merged hole to $a/m_{\text{BH}} \gtrsim 0.8$ [15], the capture of smaller companions in randomly-oriented orbits may spin down a Kerr hole instead [22].

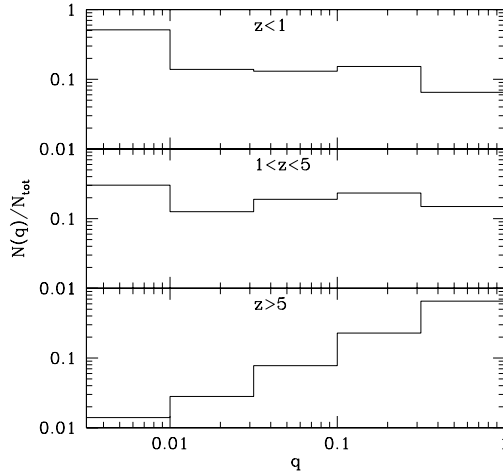


Fig. 7. Normalized distribution of mass ratios, $q = M_2/M_1$, of coalescing MBH binaries at three different epochs. Note that at low redshift MBHs typically capture much smaller companions.

In [53] we have made a first attempt at estimating the distribution of MBH spins and its evolution with cosmic time in the context of hierarchical structure formation theories, following the combined effects of black hole-black hole coalescences and accretion from a gaseous disk on the magnitude and orientation of MBH spins. Here I will briefly summarize our findings. Binary coalescences appear to cause no significant systematic spin-up or spin-down of MBHs: because of the relatively flat distribution of MBH binary mass ratios in hierarchical models (shown in Fig. 7), the holes random-walk around the spin parameter they are endowed with at birth, and the spin distribution retains significant memory of the initial rotation of “seed” holes.

It is accretion, not binary coalescences, that dominates the spin evolution of MBHs (Fig. 8). Accretion can lead to efficient spin-up of MBHs even if the angular momentum of the inflowing material varies in time. This is because, for a thin accretion disk, the hole is aligned with the outer disk on a timescale that is much shorter than the Salpeter time [37], leading to accretion via prograde equatorial orbits. As a result, most of the mass accreted by the hole acts to spin it up, even if the orientation of the spin axis changes in time. For a geometrically thick disk, alignment of the hole with the outer disk is much less efficient, occurring on a timescale comparable to the Salpeter time. Even in this case most holes will be rotating rapidly. This is because, in any model in which MBH growth is triggered by major mergers, every accretion episode must typically increase a hole’s mass by about one e-folding to account for the local MBH mass density and the $m_{\text{BH}} - \sigma_*$ relation. Most individual accretion episodes thus produce rapidly-rotating holes independent of the initial spin.

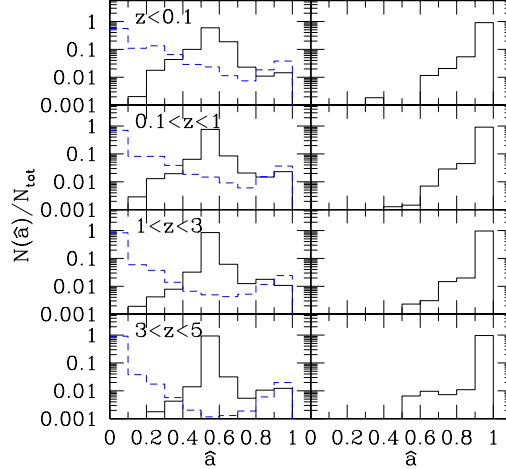


Fig. 8. Distribution of MBH spins in different redshift intervals. *Left panel:* effect of black hole binary coalescences only. *Solid histogram:* seed holes are born with $\hat{a} \equiv a/m_{\text{BH}} = 0.6$. *Dashed histogram:* seed holes are born non-spinning. *Right panel:* spin distribution from binary coalescences and gas accretion. Seed holes are born with $\hat{a} = 0.6$, and are efficiently spun up by accretion via a thin disk.

Under the combined effects of accretion and binary coalescences, we find that the spin distribution is heavily skewed towards fast-rotating Kerr holes, is already in place at early epochs, and does not change significantly below redshift 5. As shown in Figure 9, about 70% of all MBHs are maximally rotating and have mass-to-energy conversion efficiencies approaching 30%. Note that if the equilibrium spin attained by accreting MBHs is lower than the value of $\hat{a} \equiv a/m_{\text{BH}} = 0.998$ used here, as in the thick disk MHD simulations of [15], where $\hat{a} \approx 0.93$, then the accretion efficiency will be lower as well, $\approx 17\%$.

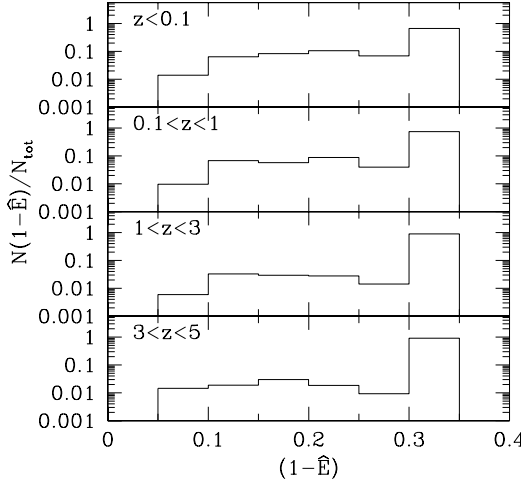


Fig. 9. Distribution of accretion efficiencies, $\epsilon \equiv 1 - \hat{E}$, in different redshift intervals (assuming that the energy radiated is the binding energy at the ISCO). The spin distribution from binary coalescences and gas accretion has been calculated assuming the holes accrete via a thin disk on prograde equatorial orbits.

Even in the conservative case where accretion is via a geometrically thick disk (and hence the spin/disk alignment is relatively inefficient) and the initial orientation between the hole's spin and the disk rotation axis is assumed to be random, we find that most MBHs rotate rapidly with spin parameters $\hat{a} > 0.8$ and accretion efficiencies $\epsilon > 12\%$. As recently shown by [56][31], a direct comparison between the local MBH mass density and the mass density accreted by luminous quasars shows that quasars have a mass-to-energy conversion efficiency $\epsilon \gtrsim 0.1$ (a simple and elegant argument originally provided by [49]). This high average accretion efficiency may suggest rapidly rotating Kerr holes, in agreement with our findings. Since most holes rotate rapidly at all epochs, our results suggest that spin is not a necessary and sufficient condition for producing a radio-loud quasar.

I would like to thank my numerous collaborators on this subject: F. Haardt, M. Kuhlen, P. Oh, E. Quataert, M. Rees, A. Sesana, and M. Volonteri. This manuscript was written while the author was enjoying the hospitality of the Kavli Institute for Theoretical Physics. Support for this work was provided by NASA grant NNG04GK85G, and by NSF grants AST-0205738 and PHY99-07949.

References

1. Abel, T., Bryan, G., & Norman, M. 2000, ApJ, 540, 39

2. Bardeen, J. M. 1970, *Nature*, 226, 64
3. Begelman, M. C., Blandford, R. D., & Rees, M. J. 1980, *Nature*, 287, 307
4. Bond, J. R., Arnett, W. D., & Carr, B. J. 1984, *ApJ*, 280, 825
5. Bromm, V., Coppi, P. S., & Larson, R. B. 1999, *ApJ*, 527, L5
6. Burkert, A., & Silk, J. 2001, *ApJ*, 554, L151
7. Cattaneo, A., Haehnelt, M. G., & Rees, M. J. 1999, *MNRAS*, 308, 77
8. Cavaliere, A., & Vittorini, V. 2000, *ApJ*, 543, 599
9. Colbert, E. J. M., & Mushotzky, R. F. 1999, *ApJ*, 519, 89
10. Ebisuzaki, T., Makino J., & Okumura S. K. 1991, *Nature*, 354, 212
11. Faber, S. M., et al. 1997, *AJ*, 114, 1771
12. Ferrarese, L., & Merritt, D. 2000, *ApJ*, 539, L9
13. Fryer, C. L., Woosley, S. E., & Heger, A. 2001, *ApJ*, 550, 372
14. Fuller, T. M., & Couchman, H. M. P. 2000, *ApJ*, 544, 6
15. Gammie, C. F., Shapiro, S. L., & McKinney, J. C. 2004, *ApJ*, 602, 312
16. Gebhardt, K., et al. 2000, *ApJ*, 543, L5
17. Haehnelt, M.G. 1994, *MNRAS*, 269, 199
18. Haehnelt, M. G., & Kauffmann, G. 2000, *MNRAS*, 318, L35
19. Haiman, Z., Abel, T., & Rees, M. J. 2000, *ApJ*, 534, 11
20. Heger, A., & Woosley, S. E. 2002, *ApJ*, 567, 532
21. Hernquist, L. 1992, *ApJ*, 400, 460
22. Hughes, S. A., & Blandford, R. D. 2003, *ApJ*, 585, L101
23. Islam, R. R., Taylor, J. E., & Silk, J. 2003, *MNRAS*, 340, 647
24. Kaaret, P., et al. 2001, *MNRAS*, 321, L29
25. Kauffmann, G., & Haehnelt, M. G. 2000, *MNRAS* 311, 576
26. Krolik, J. H. 2004, *ApJ*, in press (astro-ph/0407285)
27. Kuhlen, M., & Madau, P. 2004, in preparation
28. Machacek, M. M., Bryan, G. L., & Abel, T. 2003, *MNRAS*, 338, 273
29. Madau, P., & Rees, M. J. 2001, *ApJ*, 551, L27
30. Madau, P., Rees, M. J., Volonteri, M., Haardt, F., & Oh, S. P. 2004, *ApJ*, 606, 484
31. Marconi, A., Risaliti, G., Gilli, R., Hunt, L. K., Maiolino, R., & Salvati, M. 2004, *MNRAS*, 351, 169
32. Menou, K., Haiman, Z., & Narayanan, V. K. 2001, *ApJ*, 558, 535
33. Miller, M. C. 2004, preprint (astro-ph/0409331)
34. Miller, M. C., & Colbert, E. J. M. 2004, *Int. J. Mod. Phys. D* 13, 1
35. Milosavljevic, M., & Merritt, D. 2001, *ApJ*, 563, 34
36. Milosavljevic, M., Merritt, D., Rest, A., van den Bosch, F. C. 2002, *MNRAS*, 331, L51
37. Natarajan, P., & Pringle, J. E. 1998, *ApJ*, 506, L97
38. Oh, P. S. 2001, *ApJ*, 553, 499
39. Oh, S. P., & Haiman, Z. 2003, *MNRAS*, 346, 456
40. Oh, S. P., Nollett, K. M., Madau, P., & Wasserburg, G. J. 2001, *ApJ*, 562, L1
41. Omukai, K., & Palla, F. 2003, *ApJ*, 589, 677
42. Ricotti, M., & Ostriker, J. P. 2004, *MNRAS*, 352, 547
43. Schaefer, D. 2002, *A&A*, 382, 28
44. Schneider, R., Ferrara, A., Natarajan, P., & Omukai, K. 2002, *ApJ*, 571, 30
45. Sesana, A., Haardt, F., Madau, P., & Volonteri, M. 2004, *ApJ*, 611, 623
46. Sesana, A., Haardt, F., Madau, P., & Volonteri, M. 2004, *ApJ*, submitted (astro-ph/0409255)
47. Shull, J. M., & Van Steenberg, M. E. 1985, *ApJ*, 298, 268
48. Silk, J., & Rees, M. J. 1998, *A&A*, 331, L1

49. Soltan, A. 1982, MNRAS, 200, 115
50. Venkatesan, A., Giroux, M. L., & Shull, M. J. 2001, ApJ, 563, 1
51. Volonteri, M., Haardt, F., & Madau, P. 2003, ApJ, 582, 559
52. Volonteri, M., Madau, P., & Haardt, F. 2003, ApJ, 593, 661
53. Volonteri, M., Madau, P., Quataert, E., & Rees, M. J. 2004, ApJ, in press (astro-ph/0410342)
54. Whalen, D., Abel, T., & Norman, M. L. 2004, ApJ, 610, 22
55. Wyithe, J.S.B., & Loeb, A. 2003 ApJ, 590, 691
56. Yu, Q., & Tremaine, S. 2002, MNRAS, 335, 965